ELSEVIER

Journal of Chromatography A, 813 (1998) 313–324

JOURNAL OF CHROMATOGRAPHY A

Magnetic split-flow thin fractionation: new technique for separation of magnetically susceptible particles

C. Bor Fuh*, S.Y. Chen

Department of Applied Chemistry, Chaoyang University of Technology, 168 Gifeng East Road, Wufeng, Taichung County 413, Taiwan

Received 27 January 1998; received in revised form 30 March 1998; accepted 17 April 1998

Abstract

A magnetic split-flow thin (SPLITT) fractionation system has been constructed for the purpose of extending the capabilities of SPLITT fractionation to magnetically susceptible samples. Permanent magnets of anisotropic ferrite and Nd–Fe–B magnets were tested and used to build the magnetic field. SPLITT cells were assembled and tested for operation. The integrity and capabilities of the system were examined using silica particles, labeled silica particles and magnetic particles (Dynabeads). Particle mixtures with high and low magnetic susceptibilities were completely separated. Successful separation of particle mixtures was demonstrated using Dynabeads with glass beads, labeled silica particles with glass beads or polystyrene beads, and Dynabeads with labeled silica particles. Continuous fractionation of samples was tested for a period of 8 h using mixtures of labeled silica particles and glass beads. Fractionation was verified using magnets and light microscopy. The throughput was around 0.1 g/h with the present set-up. Sample recovery ranged from 97 to 99% with a mean of 99%. Guidelines for scaling up of this system are provided for future reference. Magnetic SPLITT fractionation shows good potential for becoming a valuable technique for separation of magnetically susceptible particles.

Keywords: Split-flow thin fractionation; Magnetic separation; Permanent magnets; Field-flow fractionation

1. Introduction

Split-flow thin (SPLITT) fractionation is a family of new techniques for separating macromolecules, colloids and particles [1–9]. SPLITT fractionation generally has two inlets, two outlets, an inlet and an outlet splitter. The inlet splitter allows smooth merging of two inlet flows, and the outlet splitter allows fractionated sample components to be collected separately without remixing. The imaginary plane for the merging of the two inlet flows is called the inlet splitting plane (ISP). The imaginary plane for the dividing of the two outlet flows is called the outlet splitting plane (OSP). Understanding of these two planes is necessary for clear understanding of SPLITT fractionation operation. The positions of the ISP and OSP are determined according to the relative flow-rates of the inlet and outlet substreams. The two main features of SPLITT fractionation are simple laminar flow and narrow (sub-mm) geometry. In SPLITT fractionation, a sample is introduced into one side of the inlet splitter, and a carrier with greater flow-rate is introduced into the other side. Sample components are compressed into a small zone below the ISP by the large flow-rate from the other side of the inlet substream when they enter the

*Corresponding author.

0021-9673/98/$19.00
PII: S0021-9673(98)00337-9

channel, as shown in Fig. 1. The ISP swerves down to a position close to the inlet splitter. Sample components are rapidly separated by field-driven migration perpendicular to the flow direction across a thin (sub-mm) layer as they pass along the SPLITT channel. Sample components with high and low mobilities are driven by the applying field perpendicular to the flow direction into various lateral positions. An outlet splitter at the outlet end of the channel divides components in different lateral positions into different outlet substreams for collection and measurement. Particles located above the OSP exit at outlet a. Particles located at or below the OSP exit at outlet b.

SPLITT fractionation is a close family of another separation technique, field-flow fractionation (FFF) [10,11]. FFF is also a family of separation techniques for macromolecules, colloids and particles. The FFF family consist of chromatographic-like elution techniques in which an external field, rather than partitioning between phases, causes differential retention. Both FFF and SPLITT fractionation use the thin separation channel and the applied perpendicular field for separation. However, the separation mechanism is different in these two techniques. In SPLITT fractionation the separation axis is the thin dimension of the channel whereas in FFF the separation axis is the flow axis. Therefore, FFF can not be run continuous like SPLITT fractionation and is not readily adaptable to preparative separations.

SPLITT fractionation is mainly designed for preparative (continuous) separation with throughput in the gram(s)- or sub-g/h range depending on the field of application [2–6]. SPLITT fractionation can also be used for analytical applications, such as rapid measurements of diffusion coefficients [12], oversized particles [13], and particle size distribution [13]. SPLITT fractionation is called ''continuous SPLITT fractionation'' when it is used for preparative applications. SPLITT fractionation is called

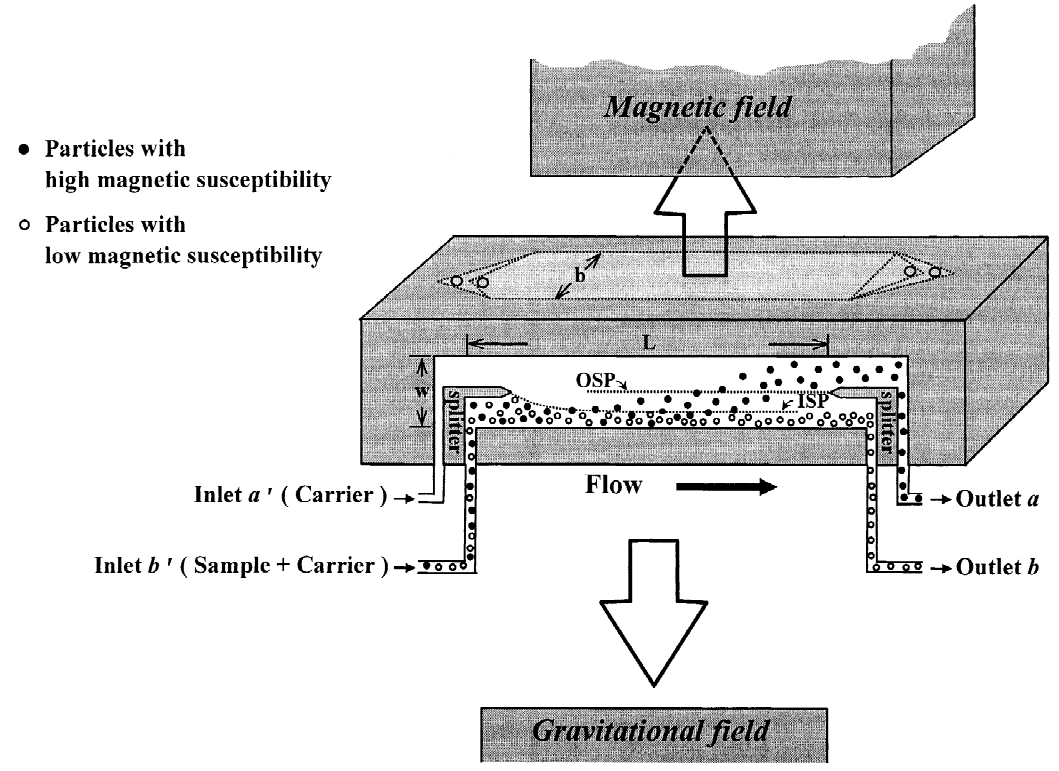

Fig. 1. Diagram of magnetic separator. Magnetic force is applied upward and gravitational force is applied downward. The flow-rate conditions: $\dot{V}(a') > \dot{V}(b')$, $\dot{V}(a) = \dot{V}(b)$, and $\dot{V}(b) > \dot{V}(b')$.

''analytical SPLITT fractionation'' when it is used for analytical applications.

The selectivity of SPLITT fractionation comes from the applied force. The applied forces currently used for SPLITT fractionation are gravitational forces, centrifugal forces, electrical forces, concentration gradients and hydrodynamic lift forces [1–9]. Developing other applied forces as separation bases as well as extending the selectivity and applications of the present ones is very important for SPLITT fractionation. It is especially urgent to increase the selectivity of SPLITT fractionation to meet the increasing demands for separation techniques to deal with challenging samples. Magnetic separation is fast and selective for magnetically susceptible samples. Therefore, magnetic separation is a good candidate for investigation. Magnetic fields with permanent magnets are especially simple and economical to use and deserve development and investigation.

In this study we first evaluated magnetic fields using various magnetic assembles. We then tested and characterized the integrity of separation channel using standard latexes. Finally, we demonstrated successful separation with this system using particle mixtures.

2. Theory

Experiments were done using the system set-up shown in Fig. 1. The system had two inlets, two outlets, an inlet and an outlet splitter. The theory of operation of system is similar to that of other SPLITT systems applied in various fields [3,13]. Magnetic force and gravitational force were applied in opposite direction on the channel to facilitate separation by the set-up. Sample components with carriers were introduced into inlet b′ and the sample-free carriers were introduced into inlet a′ to confine the samples into a small zone close to the bottom wall of the channel. Magnetic force drove the particles with high magnetic susceptibility (shown as solid circles in the figure) upward toward the top wall, while sample components passed along the channel below. Particles with low magnetic susceptibility (shown as hollow circles in the figure) settled toward the bottom wall due to gravitational force. Particles with high magnetic susceptibility came out at outlet a, and particles with low magnetic susceptibility came out at outlet b. The particles with high magnetic susceptibilities tended to exit at outlet a when magnetically induced flow-rates were high enough, while particles with low magnetic susceptibilities tended to exit at outlet b when magnetically induced flow-rates were low enough.

For a species to be transported across a lamina of flow-rate $\dot{V}_i$, the field-induced flow-rate (bLU) must be larger than or equal to $\dot{V}_i$, as shown in the following equation [2]:

$$bLU \geq \dot{V}_i \tag{1}$$

where b is the channel breadth, L is the channel length, and U is the field-induced velocity. All particles with high magnetic susceptibility exit at outlet a when Eq. (2) is satisfied. This means that the net flow-rate resulting from subtracting the magnetically-induced flow-rate (bLU_m) from the gravitationally-induced flow-rate (bLU_g) was higher than the flow-rate at outlet b. Similarly all particles with low magnetic susceptibilities exit at outlet b when Eq. (3) is satisfied. The requirement that particles with very low magnetic susceptibility are fully retrieved at outlet b is quite straightforward from Eq. (3) when $\dot{V}(b) > \dot{V}(b')$ (i.e., the volumetric flow-rate at outlet b is higher than that at inlet b′). The gravitationally-induced flow-rate does not play an important role for particles with very low magnetic susceptibilities as shown in Eq. (3). The conditions of flow-rate used in this study kept $\dot{V}(b) > \dot{V}(b')$ valid. In order to have complete separation, Eqs. (2) and (3) must both be satisfied by particles with high and low magnetic susceptibilities

$$bLU_{mh} - bLU_g \geq \dot{V}(b) \tag{2}$$

$$bLU_{ml} - bLU_g < \dot{V}(b) - \dot{V}(b') \tag{3}$$

All particles with high magnetic susceptibilities exit at outlet a when Eq. (2) is satisfied. All particles with low magnetic susceptibilities exit at outlet b when Eq. (3) is satisfied.

Where U_m is the magnetically-induced velocity (U_{mh} and U_{ml} are used for magnetically-induced velocities of particles with high and low magnetic susceptibilities, respectively), U_g is the gravitationally-induced velocity, $\dot{V}(b)$ is the volu-

metric flow-rate at outlet b, and $\dot{V}(b')$ is the volumetric flow-rate at inlet b′. Magnetically-induced velocity, U_m, can be calculated using [14]

$$U_m = \frac{\Delta\chi \Delta H^2 d}{48\eta} \quad (4)$$

where $\Delta\chi = \chi_p - \chi_c$, χ_p and χ_c are the respective magnetic susceptibilities of particles and carriers, η is the fluid viscosity, d is the spherical particle diameter or the effective spherical diameter, and symbol ΔH is the drop in magnetic field strength. Gravitationally-induced velocity, U_g, can be calculated using

$$U_g = \frac{\Delta\rho d^2 g}{18\eta} \quad (5)$$

where η is the fluid viscosity, $\Delta\rho$ is the particle density minus the carrier fluid density, g is gravitational acceleration, and d is the spherical particle diameter or the effective spherical diameter. For particles with magnetically-induced velocity U_m is between U_{mh} and U_{ml} i.e., $\dot{V}(b) - \dot{V}(b') \leq bLU_m - bLU_g < \dot{V}(b)$, the fraction of particles exiting at outlet a could be calculated using:

$$\frac{bLU_m - bLU_g - \dot{V}(b) + \dot{V}(b')}{\dot{V}(b')} \quad (6)$$

3. Experimental

The channel length, breadth and thickness used were 10 cm, 0.5 cm and 0.025 cm, respectively. The calculated void volume was 0.125 ml. The volume of the injection loop was equal to 0.5 ml when the system was used for testing and optimization. The channel components are shown in Fig. 2. The channel consisted of three layers of cut-out Mylar with the ends of the center piece used as the inlet and outlet splitters. All layers were then sandwiched together between sheets of plastic, which served as the channel walls.

Magnetic fields were generated by a permanent magnet assembly consisting of one pair of anisotropic ferrite magnets and rare earth magnets (Nd–Fe–B). The magnets were connected by soft iron pole pieces, which conducted the magnetic flux lines to the interpolar gap. The anisotropic ferrite magnets, characterized by a maximum energy product of $4.0 \cdot 10^6$ gauss-oersteds, and the Nd–Fe–B (neodymium–iron–boron) magnets, characterized by a maximum energy product of $3.0 \cdot 10^7$ gauss-oersteds were obtained from Super Electronics (Taipei, Taiwan). Nd–Fe–B magnets were used for most characterization of the separation channel. Magnetic field strengths generated by various gap widths were measured for use as references for the magnetic field assemblies. A gap width of 5 mm was used for most experiments unless otherwise indicated. The gap length was 10 cm. The magnetic field measurements were made using a Gaussmeter and a Hall effect probe (Model Gauss MG-7D, Walker Scientific, Worcester, MA, USA). The probe measured magnetic flux perpendicular to a sensing area with a diameter of 6.94 mm. The polar coordinates (r, θ) with (0, 0) located at the center of the gap was used for measurement of magnetic field, as shown in Fig. 3. The combined magnets and pole pieces have geometrical size of 17.5 cm × 10 cm × 6.0 cm and weights of 5.5 kg. The distance between channel and magnetic gap was optimized for various flow-rates and particles with various magnetic susceptibilities.

An LC pump (SSI series II, State College, PA, USA), and micro-tubing pumps (Eyela Mp-3, Rikakikai, Tokyo, Japan) were used to deliver samples and carriers into the separation channel. Light microscopy (Olympus BX-50, Tokyo, Japan) was used for particle verification. A hemacytometer was used to count particles. Silica particles (1–10 μm) and iron nitrate were purchased from Sigma (St. Louis, MO, USA). Erbium chloride was obtained from Strem (Newsburyport, MA, USA). Dynabeads M-450 of 4.5 μm were obtained from Dynal (Lake Success, NY, USA). Glass beads of 1–5 μm and polystyrene beads of 5 μm were obtained from Duke Scientific (Palo Alto, CA, USA).

The carrier composition used for silica and erbium-labeled particles was 0.10 *M* carbonate buffer with pH equal to 7.8. Labeled silica particles were prepared using opposite charge attraction between positively charged iron (or erbium) ions and negatively charged silica surface. They were mixed, incubated for 60 min and then washed with pH 7.8 carbonate buffer three times before use. Iron-labeled silica particles were purified before experimental use in particle mixture separation by removing particles

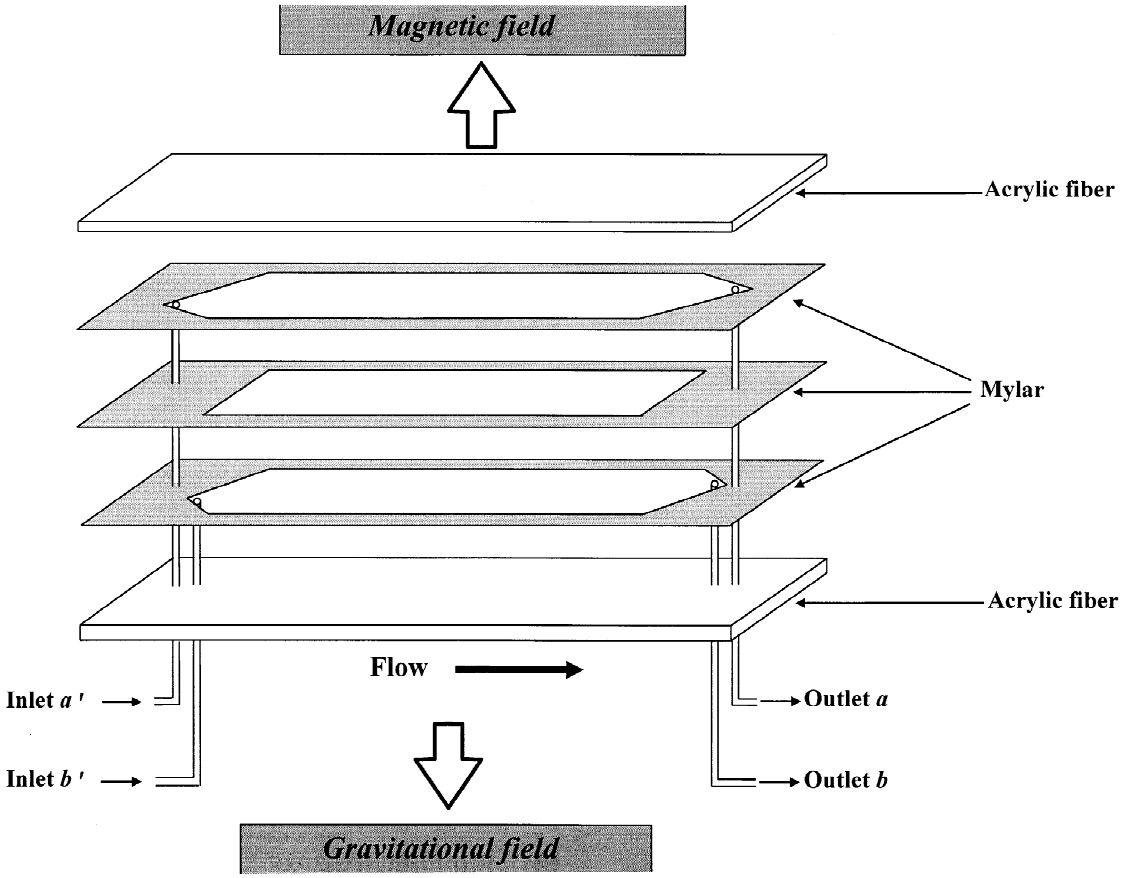

Fig. 2. Components of magnetic separator. Two inlets (inlet a′ and inlet b′) and two outlets (outlet a and outlet b) are shown. The two edges of centered Mylar are used for inlet and outlet splitters.

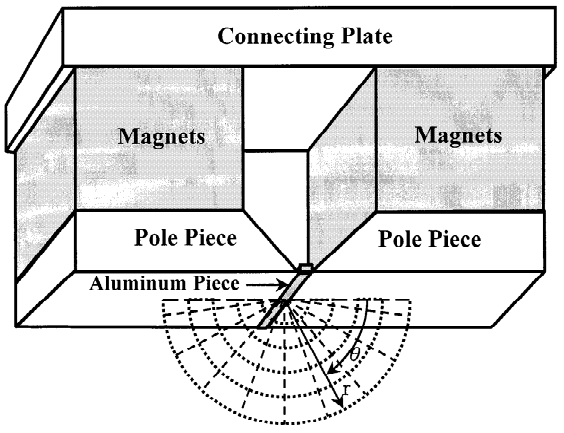

Fig. 3. Components of magnetic field. An aluminum piece was used as the gap between two pole pieces.

not well-labeled via the SPLITT channel. The experimental conditions for this purification were $\dot{V}(a')=3.6$, $\dot{V}(b')=1.2$, $\dot{V}(a)=2.4$, $\dot{V}(b)=2.4$ ml/min.

The fractional retrieval at outlet a (F_a) was calculated using the following equation:

$$F_a = \frac{N_a}{N_a + N_b} \quad (7)$$

where N_a is the number of silica particles exiting at outlet a, and N_b is the number of silica particles exiting at outlet b. The percentage recovery of labeled silica particles was calculated by adding the total number of labeled silica particles exiting at outlets a and b, and dividing by the total number of labeled silica particles entering at the inlets. Pulsed sample injection with a loop volume of 0.5 ml was

used in the experiments of recovery and fractional retrieval.

4. Results and discussion

The magnetic fields from different magnets were measured for comparison, as shown in Fig. 4. The magnetic fields were plotted against the polar coordinates radii at $\theta = 90°$. Fig. 4 clearly shows that Nd–Fe–B magnets provide higher magnetic field strength than ferrite magnets of similar size, especially when the working distance is within a radius of 5 mm. Fig. 4 also shows that the maximum magnetic field is located around 2.5 mm below the gap surface ($r < 0$). The consistency of magnetic field along the gap length was tested by measuring magnetic field at a radius of 3.5 mm. The magnetic field along the gap length was quite consistent, which was necessary for our experiments. The magnetic field only dropped about 10% when the gap was around 10 mm from the gap edges, and variations in the magnetic field over the rest of gap length was less than 3%. The surfaces of the pole pieces near the gap may be considered equipotential surfaces [15,16]. The magnetic field was approximately inversely proportional to the radius at distances greater than the gap width. Magnetic field strength plotted against the inverse of radial distance shows good fitting of linear relationship (within $r = 5$ mm), as shown in Fig. 5. Deviation from the linear relationship gradually increases as the $1/r$ value becomes greater than 0.2. Magnetic field strength plotted against various angles (θ) at various radial distances are shown in Fig. 6. Magnetic fields showed more consistency at similar radial distances at various angles when the radial distances were greater, as shown in Fig. 6. This result also agrees well with equipotential surface theory [15,16]. The effects of various gap widths on magnetic field

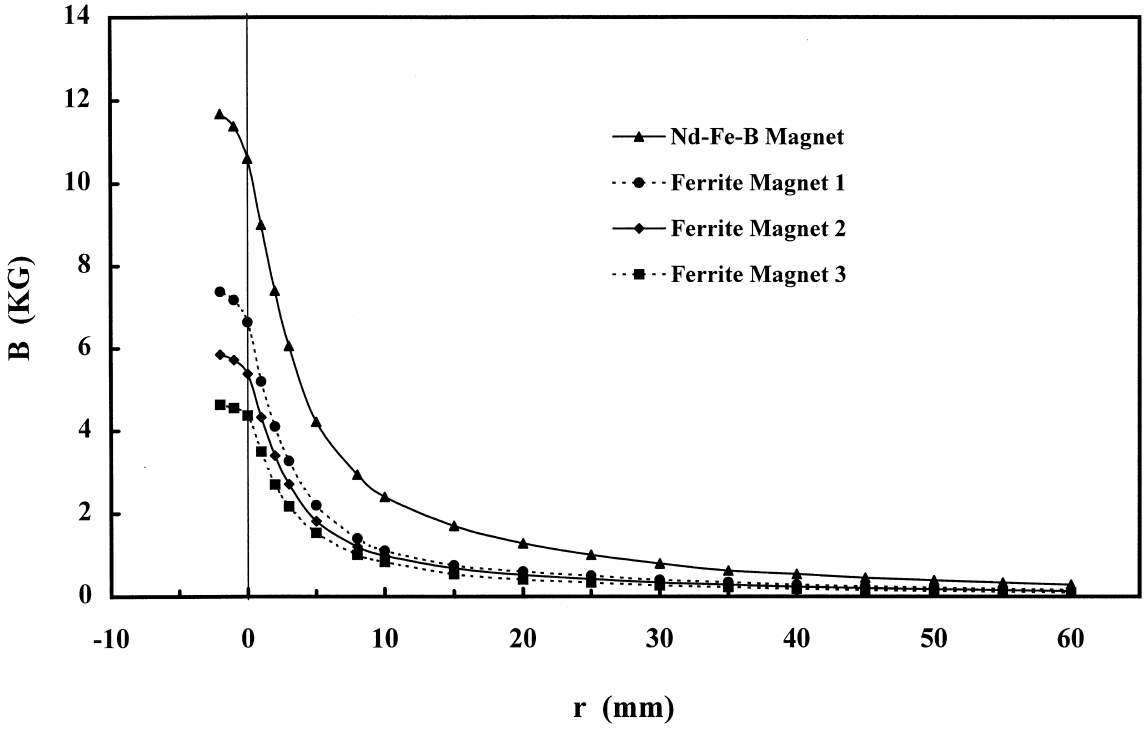

Fig. 4. Magnetic field as a function of radius for different magnets at $\theta = 90°$, ND–Fe–B magnets: length = 10 cm, width = 5 cm, height = 2.54 cm; ferrite magnets: (1) anisotropy, length = 10 cm, width = 7.5 cm, height = 5.08 cm; (2) anisotropy, length = 10 cm, width = 7.5 cm, height = 2.54 cm; (3) anisotropy, length = 10 cm, width = 5.0 cm, height = 2.54 cm.

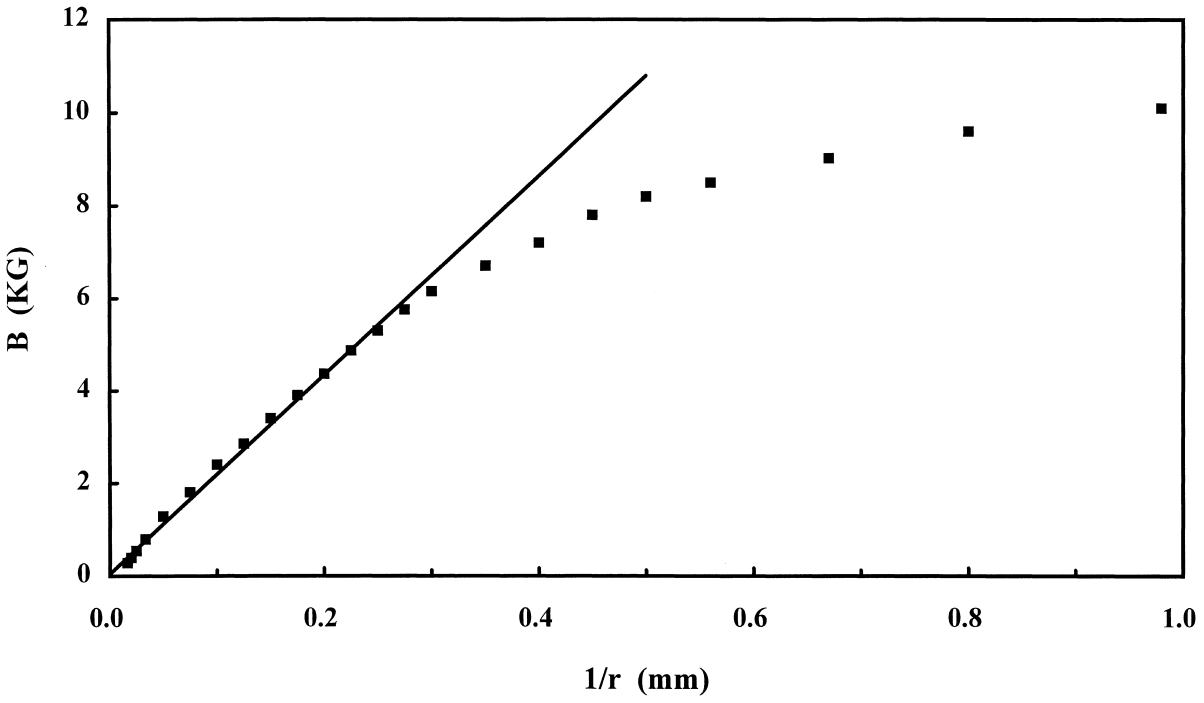

Fig. 5. Magnetic field of Nd–Fe–B magnets as a function of $1/r$ at $\theta=0$. The linear regression of magnetic field (B) on $1/r$ within $1/r$ of 0.25, slope = 21.52, intercept = 0.04, and $r^2=0.99$.

strength as a function of radius at $\theta=90°$ are shown in Fig. 7. The magnetic field strength was higher when the gap width was smaller at a fixed distance closing to the gap surface. We needed large enough gap width to apply magnetic forces homogeneously on the channel in these experiments. We also needed strong magnetic fields for these experiments. A gap width of 5 mm was chosen for use in most experiments as trade-off between large gap width and strong magnetic field.

Labeled silica particles (labeled with iron and erbium cations) were used to test and characterize the channel assembly of the system set-ups. The fractional retrieval at outlet a (F_a) was used to express the results of characterization. The F_a was equal to one (100%) when all particles exited at outlet a. The F_a was equal to zero when all particles exited at outlet b. The results of fractional retrieval experiments using iron- and erbium-labeled silica particles are shown in Table 1. The optimal distances between channel and gap surface were a little larger for erbium-labeled silica particles than for iron-labeled silica particles, meaning that the magnetic susceptibility of erbium-labeled silica particles is a little higher than that of iron-labeled silica particles. The results of fractional retrieval were all close to 100% for both erbium- and iron-labeled silica particles. Magnetic field strengths were high enough to drive magnetically susceptible silica particles to exit at outlet a, satisfying Eq. (2). The F_a from reinjection of fractionatedly labeled silica particles was equal to 100% at various flow-rates. This suggests that most silica particles are well-labeled. Poorly labeled silica particles were removed using the SPLITT system before experiments of particle mixture separation. The F_a of unlabeled silica particles, all equal to zero, were used as references. These experiments confirm the workability of magnetic SPLITT fractionation, and also show that charge labeling of silica particles is quite effective.

The recovery for labeled silica particles in the separation channel is shown in Table 2. The average recovery for labeled silica particles was 98.9%. The average recovery for Dynabeads and glass beads was

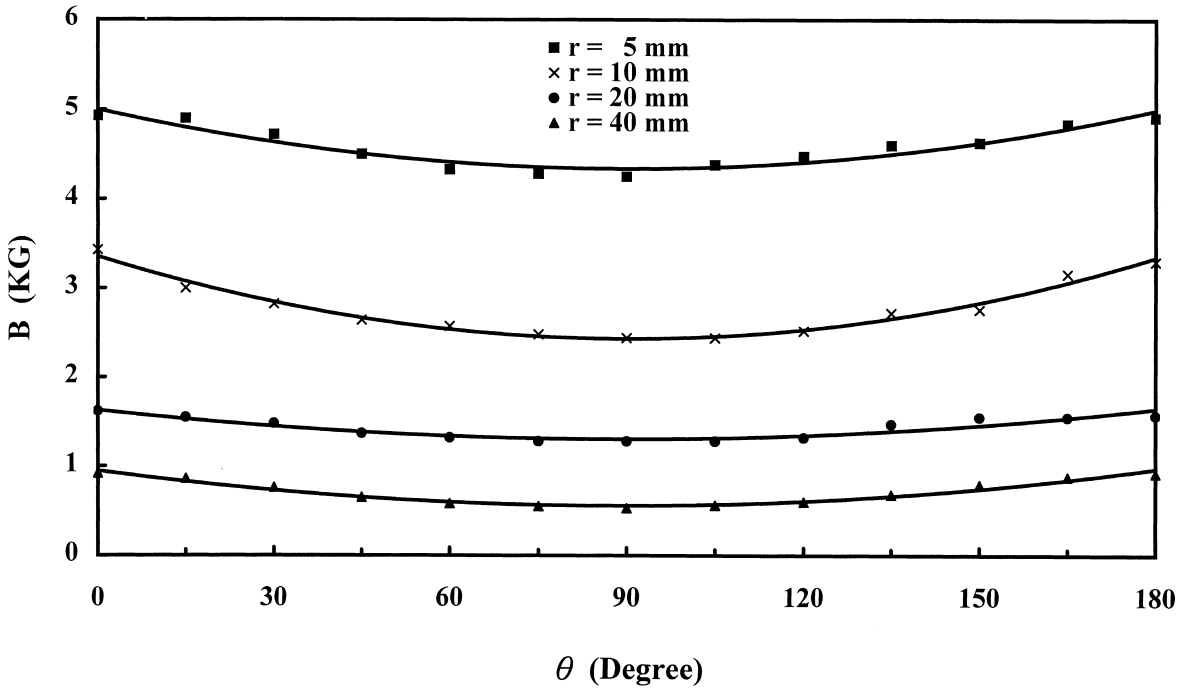

Fig. 6. Magnetic field of Nd–Fe–B magnets around the interloper gap as a function of position in polar coordinates [r, θ].

97.1% and 99.4%, respectively (results not shown). Good recovery for different samples suggest that very few samples were lost in the fractionation process. The system set-up was also characterized using magnetic particles (Dynabeads). The F_a results for Dynabeads are shown in Table 3. The F_a of Dynabeads were all equal to 100%, meaning that all Dynabeads were retrieved at outlet a. The optimal distances between channel and gap surface of magnets for Dynabeads were much greater than those used for labeled silica particles. This suggests that Dynabeads have higher magnetic susceptibility than labeled silica particles. This is reasonable since the Dynabeads used were doped with magnetite at 23% (w/v), whereas, we labeled only the surface areas of the silica particles.

Successful separation of particle mixtures was demonstrated using Dynabeads with glass beads, labeled silica particles with glass beads or polystyrene latex beads, and Dynabeads with labeled silica particles. The magnetically susceptible particles (Dynabeads or labeled silica particles) were first injected into the SPLITT channel to insure that they were fully retrieved at outlet a ($F_a = 100\%$). This confirmed that the magnetic force was strong enough to drive magnetically susceptible particles upward to pass the OSP and exit at outlet a. The magnetically unsusceptible particles (glass beads or polystyrene latex beads) were then injected into SPLITT channel to insure that they were fully retrieved at outlet b ($F_a = 0$). This conditions of $F_a = 0$ was easily satisfied due to the negligible magnetic force and flow-rate conditions we chose. Finally mixtures of magnetically susceptible and unsusceptible particles were then introduced into the channel for separation. The fractionated products at outlets a and b were collected and their purities were checked with magnets and microscopy. The F_a for labeled silica particles with low magnetic susceptibility and glass and polystyrene beads with trace magnetic susceptibilities are shown in Table 4. The optimal distance for labeled silica particles was used in this experimental separation. Particles with trace magnetic susceptibilities satisfied Eq. (3), and were fully retrieved at outlet b ($F_a = 0$). Particles with low magnetic susceptibilities were fully retrieved at

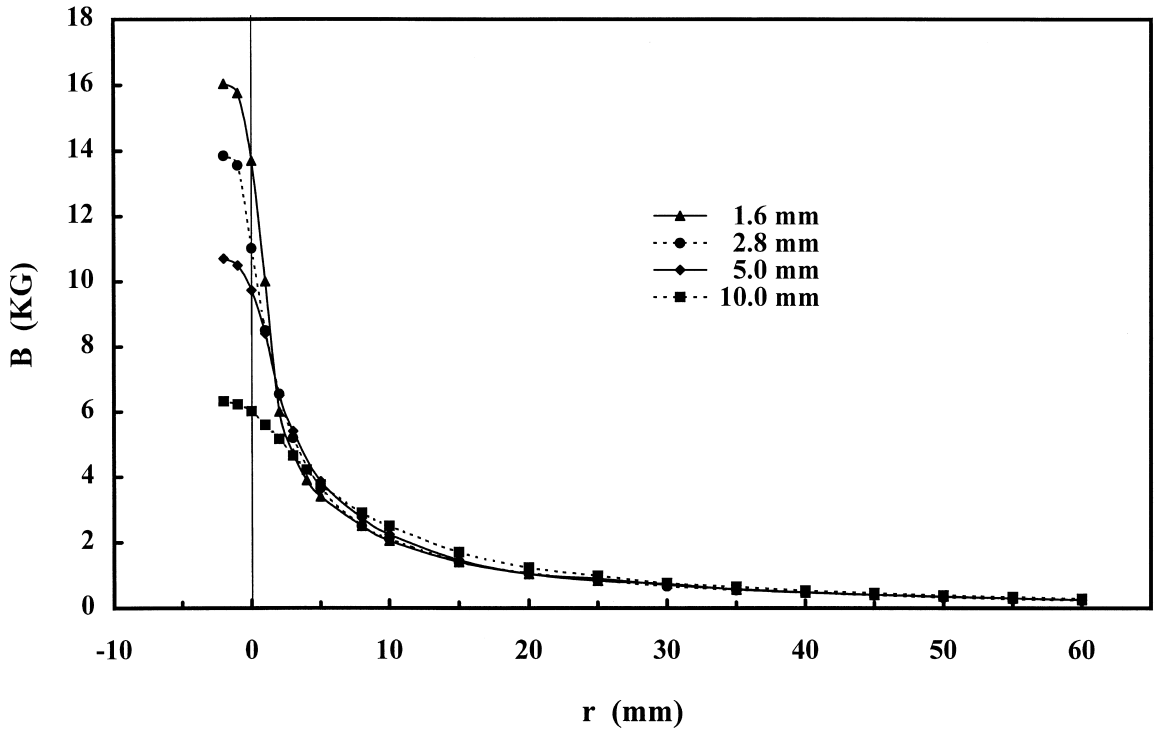

Fig. 7. Magnetic field of Nd–Fe–B magnets as a function of radius for different gap widths at $\theta = 90°$.

outlet a with sufficient magnetically induced velocity. The particles with high magnetic susceptibilities (Dynabeads) were also successfully separated from particles with low magnetic susceptibilities (labeled silica particles) in the same way, as shown in Table 3. Labeled silica particles did not have sufficient $\Delta\chi$ values for magnetically-induced velocity (bLU_m), and were all retrieved at outlet b at optimal distance for Dynabeads. On the other hand, Dynabeads with high enough bLU_m terms to satisfy Eq. (2) were fully retrieved at outlet a under the same conditions.

Finally, continuous separation of iron-labeled silica particles from glass beads was run unattended at a flow-rate of 3.2 ml/min for 8 h. The flow-rate conditions were $\dot{V}(a') = 2.4$, $\dot{V}(b') = 0.8$, $\dot{V}(a) = 1.6$, $\dot{V}(b) = 1.6$ ml/min. The fractionated particles were found to be not contaminated by each other during fractionation when checked using magnets and microscopy. The throughput was around 0.1 g/h with the present set-up. The throughput was proportional to cell area bL, magnetic susceptibility differences among particles and carriers, and the square of the magnetic field drop according to theory [3]. This suggests that larger difference in magnetic susceptibilities between particles and carriers, greater gap length and widths, and higher magnetic fields would yield larger throughputs. The choice of gap width involves a trade-off with magnetic field strength, as shown in Fig. 6. Larger gap widths would have lower magnetic field strengths at working distances closer to the gap surface. Longer gap lengths with higher magnetic fields is the best way to increase the throughput. The gap length can easily be increased by several times using this set-up. The magnetic field can also be increased several times by using superconducting magnets. These improvements would increase the throughput of the present system by an order of magnitude.

Magnetic SPLITT fractionation extends the capabilities of SPLITT fractionation to magnetically susceptible particles. The selectivity of magnetic SPLITT fractionation complements that of commonly used SPLITT techniques such as sedimentation

Table 1
Fractional retrieval at outlet a (F_a) of erbium-labeled and iron-labeled silica particles

Sample	Inlet concentration (No./ml)	Inlet flow-rate (ml/min)		Outlet flow ratio [$\dot{V}$(a)/$\dot{V}$(b)]	F_a (%)	F_a for rejection (%)
		$\dot{V}$(a′)	$\dot{V}$(b′)			
SiO_2 labeled with Er^{3+}	$1.12\cdot10^6$	1.2[a]	0.4	1	99.78	100
	$1.12\cdot10^7$			1	99.85	100
	$1.12\cdot10^6$	2.4[b]	0.8	1	99.76	100
	$1.12\cdot10^7$			1	99.11	100
	$1.12\cdot10^6$	3.6[c]	1.2	1	99.76	100
	$1.12\cdot10^7$			1	99.85	100
SiO_2 labeled with Fe^{3+}	$1.23\cdot10^6$	1.2[d]	0.4	1	99.83	100
	$1.23\cdot10^7$			1	99.84	100
	$1.23\cdot10^6$	2.4[e]	0.8	1	99.82	100
	$1.23\cdot10^7$			1	99.85	100
	$1.23\cdot10^6$	3.6[f]	1.2	1	99.75	100
	$1.23\cdot10^7$			1	99.87	100
SiO_2	$1.12\cdot10^6$	1.2	0.4	1	0	–
	$1.12\cdot10^7$			1	0	–
	$1.12\cdot10^6$	2.4	0.8	1	0	–
	$1.12\cdot10^7$			1	0	–
	$1.12\cdot10^6$	3.6	1.2	1	0	–
	$1.12\cdot10^7$			1	0	–

The optimized distance between channel and magnetic gap: [a] =4.00 mm, [b] =1.60 mm, [c] =0.80 mm, [d] =3.90 mm, [e] =1.50 mm, [f] =0.75 mm.

Table 2
Recovery of erbium-labeled and iron-labeled silica particles

Sample	Inlet concentration (No./ml)	Inlet flow-rate (ml/min)		No. of sample at inlet b′	No. of sample at outlets a	No. of sample at outlets b	Recovery (%)
		$\dot{V}$(a′)	$\dot{V}$(b′)				
SiO_2 labeled with Er^{3+}	$1.12\cdot10^6$	1.2[a]	0.4	$5.60\cdot10^5$	$5.56\cdot10^5$	$1.25\cdot10^3$	99.51
	$1.12\cdot10^7$			$5.60\cdot10^6$	$5.55\cdot10^6$	$8.12\cdot10^3$	99.25
	$1.12\cdot10^6$	2.4[b]	0.8	$5.60\cdot10^5$	$5.54\cdot10^5$	$1.31\cdot10^3$	99.16
	$1.12\cdot10^7$			$5.60\cdot10^6$	$5.55\cdot10^6$	$9.57\cdot10^3$	99.28
	$1.12\cdot10^6$	3.6[c]	1.2	$5.60\cdot10^5$	$5.48\cdot10^5$	$1.30\cdot10^3$	98.09
	$1.12\cdot10^7$			$5.60\cdot10^6$	$5.46\cdot10^6$	$8.20\cdot10^3$	97.65
SiO_2 labeled with Fe^{3+}	$1.23\cdot10^6$	1.2[d]	0.4	$6.15\cdot10^5$	$6.09\cdot10^5$	$1.03\cdot10^3$	99.19
	$1.23\cdot10^7$			$6.15\cdot10^6$	$6.12\cdot10^6$	$9.56\cdot10^3$	99.67
	$1.23\cdot10^6$	2.4[e]	0.8	$6.15\cdot10^5$	$6.10\cdot10^5$	$1.11\cdot10^3$	99.37
	$1.23\cdot10^7$			$6.15\cdot10^6$	$6.12\cdot10^6$	$8.95\cdot10^3$	99.66
	$1.23\cdot10^6$	3.6[f]	1.2	$6.15\cdot10^5$	$6.03\cdot10^5$	$1.50\cdot10^3$	98.29
	$1.23\cdot10^7$			$6.15\cdot10^6$	$6.02\cdot10^6$	$7.90\cdot10^3$	98.01

The optimized distance between channel and magnetic gap: [a] =4.00 mm, [b] =1.60 mm, [c] =0.80 mm, [d] =3.90 mm, [e] =1.50 mm, [f] =0.75 mm.

Table 3
Fractional retrieval at outlet a (F_a) of Dynabeads M-450, iron-labeled silica particles and glass beads

Sample	Inlet concentration (No./ml)	Inlet flow-rate (ml/min)		Outlets flow ratio [$\dot{V}$(a)/$\dot{V}$(b)]	F_a (%)
		$\dot{V}$(a′)	$\dot{V}$(b′)		
Dynabeads M-450	$1\cdot10^6$	1.2[a]	0.4	1	100
	$1\cdot10^7$			1	100
	$1\cdot10^6$	2.4[b]	0.8	1	100
	$1\cdot10^7$			1	100
	$1\cdot10^6$	3.6[c]	1.2	1	100
	$1\cdot10^7$			1	100
SiO_2 labeled with Fe^{3+}	$1.23\cdot10^6$	1.2[a]	0.4	1	0
	$1.23\cdot10^7$			1	0
	$1.23\cdot10^6$	2.4[b]	0.8	1	0
	$1.23\cdot10^7$			1	0
	$1.23\cdot10^6$	3.6[c]	1.2	1	0
	$1.23\cdot10^7$			1	0
Glass beads	$1.1\cdot10^6$	1.2[a]	0.4	1	0
	$1.1\cdot10^7$			1	0
	$1.1\cdot10^6$	2.4[b]	0.8	1	0
	$1.1\cdot10^7$			1	0
	$1.1\cdot10^6$	3.6[c]	1.2	1	0
	$1.1\cdot10^7$			1	0

The optimized distance between channel and magnetic gap: [a] = 39.4 mm, [b] = 28.6 mm, [c] = 25.0 mm.

Table 4
Fractional retrieval at outlet a (F_a) of iron-labeled silica particles, polystyrene and glass beads

Sample	Inlet concentration (No./ml)	Inlet flow-rate (ml/min)		Outlets flow ratio [$\dot{V}$(a)/$\dot{V}$(b)]	F_a (%)	F_a for rejection (%)
		$\dot{V}$(a′)	$\dot{V}$(b′)			
SiO_2 labeled with Fe^{3+}	$1.23\cdot10^6$	1.2[a]	0.4	1	99.83	100
	$1.23\cdot10^7$			1	99.84	100
	$1.23\cdot10^6$	2.4[b]	0.8	1	99.82	100
	$1.23\cdot10^7$			1	99.85	100
	$1.23\cdot10^6$	3.6[c]	1.2	1	99.75	100
	$1.23\cdot10^7$			1	99.87	100
Glass beads	$1.1\cdot10^6$	1.2[a]	0.4	1	0	–
	$1.1\cdot10^7$			1	0	–
	$1.1\cdot10^6$	2.4[b]	0.8	1	0	–
	$1.1\cdot10^7$			1	0	–
	$1.1\cdot10^6$	3.6[c]	1.2	1	0	–
	$1.1\cdot10^7$			1	0	–
Polystyrene	$1.2\cdot10^6$	1.2[a]	0.4	1	0	–
	$1.2\cdot10^7$			1	0	–
	$1.2\cdot10^6$	2.4[b]	0.8	1	0	–
	$1.2\cdot10^7$			1	0	–
	$1.2\cdot10^6$	3.6[c]	1.2	1	0	–
	$1.2\cdot10^7$			1	0	–

The optimized distance between channel and magnetic gap: [a] = 3.90 mm, [b] = 1.50 mm, [c] = 0.75 mm.

and electric SPLITT fractionation. Magnetic SPLITT fractionation can separate particles of the similar sizes and densities with different magnetic susceptibilities which is extremely difficult using existing SPLITT fractionation techniques.

5. Conclusions

This study provides an initial evaluation of magnetic SPLITT fractionation and demonstrates its effectiveness in fractionating highly magnetically susceptible particles from less highly magnetically susceptible and magnetically unsusceptible particles. Particles with low magnetic susceptibilities can also be successfully separated from particles having trace magnetic susceptibilities. Magnetic SPLITT fractionation with permanent magnets provides simple, selective and economical separation of magnetically susceptible particles. Magnetic SPLITT fractionation can become a valuable separation technique for separation of magnetically susceptible particles.

Acknowledgements

This work was supported by grant NSC-86-2113-M-324-002 from National Science Council of Taiwan.

References

[1] J.C. Giddings, Sep. Sci. Technol. 20 (1985) 749.
[2] S.R. Springston, M.N. Myers, J.C. Giddings, Anal. Chem. 59 (1987) 344.
[3] C.B. Fuh, M.N. Myers, J.C. Giddings, Ind. Eng. Chem. Res. 33 (1994) 355.
[4] J.C. Giddings, Sep. Sci. Technol. 23 (1988) 119.
[5] C.B. Fuh, J.C. Giddings, Sep. Sci. Technol. 32 (1997) 2945.
[6] Y. Gao, M.N. Myers, B.N. Barman, J.C. Giddings, Part. Sci. Technol. 9 (1991) 105.
[7] J.C. Giddings, Sep. Sci. Technol. 27 (1992) 1489.
[8] J.C. Giddings, Sep. Sci. Technol. 23 (1988) 931.
[9] P.S. Williams, S. Levin, T. Lenczycki, J.C. Giddings, Ind. Eng. Chem. Res. 31 (1992) 2172.
[10] J.C. Giddings, Science 260 (1993) 1456.
[11] K.D. Caldwell, Anal. Chem. 60 (1988) 959A.
[12] C.B. Fuh, S. Levins, J.C. Giddings, Anal. Biochem. 208 (1993) 80.
[13] C.B. Fuh, M.N. Myers, J.C. Giddings, Anal. Chem. 64 (1992) 3125.
[14] T.M. Vickrey, J.A. Garcia-Ramirez, Sep. Sci. Technol. 15 (1980) 1297.
[15] E. Weber, Electromagnetic Fields – Theory and Applications, Vol. 1: Mapping of Fields, Wiley, New York, 1960, Ch. 7.
[16] E.M. Purcell, Electricity and Magnetism, McGraw Hill, New York, 1985, Ch. 6.